# Global (volume-averaged) model of inductively coupled chlorine plasma : influence of Cl wall recombination and external heating on continuous and pulse-modulated plasmas

Global (volume-averaged) model of inductively coupled chlorine plasma: Influence of Cl wall recombination and external heating on continuous and pulse-modulated plasmas



2014 Plasma Sources Sci. Technol. 23 045002

(http://iopscience.iop.org/0963-0252/23/4/045002)

IOP Publishing Plasma Sources Science and Technology

Plasma Sources Sci. Technol. **23** (2014) 045002 (14pp) doi:10.1088/0963-0252/23/4/045002

# Global (volume-averaged) model of inductively coupled chlorine plasma: Influence of Cl wall recombination and external heating on continuous and pulse-modulated plasmas

**Efe Kemaneci[1], Emile Carbone[1,2], Jean-Paul Booth[3], Wouter Graef[1], Jan van Dijk[1] and Gerrit Kroesen[1]**

[1] Department of Applied Physics, Eindhoven University of Technology, P O Box 513, 5600 MB Eindhoven, The Netherlands
[2] Univ. Grenoble Alpes , CNRS, CEA-Leti Minatec, LTM, F-38054 Grenoble Cedex, France
[3] LPP, CNRS, Ecole Polytechnique, UPMC, Paris XI, 91128 Palaiseau, France

E-mail: efekemaneci@gmail.com

Received 12 March 2014, revised 17 April 2014
Accepted for publication 14 May 2014
Published 12 June 2014

**Abstract**

An inductively coupled radio-frequency plasma in chlorine is investigated via a global (volume-averaged) model, both in continuous and square wave modulated power input modes. After the power is switched off (in a pulsed mode) an ion–ion plasma appears. In order to model this phenomenon, a novel quasi-neutrality implementation is proposed. Several distinct Cl wall recombination probability measurements exist in the literature, and their effect on the simulation data is compared. We also investigated the effect of the gas temperature that was imposed over the range 300–1500 K, not calculated self-consistently. Comparison with published experimental data from several sources for both continuous and pulsed modes shows good agreement with the simulation results.

Keywords: plasma physics, atomic and molecular physics, chemical physics and physical chemistry

(Some figures may appear in colour only in the online journal)

## 1. Introduction

Chlorine-based inductively coupled plasmas are widely used for surface etching in the fabrication of microelectronics [1]. The low dissociation energy of chlorine leads to significant dissociation rates in these plasmas. Moreover, the large electron affinity of atomic chlorine leads to high degrees of electronegativity. In applications a wide range of operation parameters is used, with a pressure range 1–100 mTorr and power input variation within 100–1000 W. Furthermore, the power is applied either continuously or in a modulated mode, with periods in the microsecond [2, 3] or millisecond time-scales [4]. The use of pulsed plasmas allows different process regimes to be accessed, in which the gas fragmentation and the reactive neutral to ion flux ratios to the substrate can be controlled.

Chlorine atoms can only recombine to form $Cl_2$ molecules at the chamber walls, with a rate that is described by a wall recombination probability. This process has a major effect on the atomic and molecular chlorine densities in the plasma. This recombination rate has been measured by several groups, which have shown that it can depend on numerous parameters such as the atomic to molecular chlorine density ratio [5], the gas temperature [6], the pressure [7], the wall material [6, 8],

 

and even the surface coating history [9]. The role of the recombination probability has been studied via models by Lee *et al* [10] and is further discussed by Meeks *et al* [11] with experimental comparisons. However, a detailed discussion is mostly absent and an up to date analysis is necessary due to recent improvements in the chemical kinetics [5, 12, 13]. The gas temperature is another parameter that can have a major effect on the plasma characteristics due to its impact on the gas density, the volume chemical reaction rates and the interactions at the plasma boundary. Nonetheless, the plasma sensitivity to a gas temperature variation has not been analysed up to now. In this study, we address these issues by providing a detailed analysis of the plasma response with respect to the recombination probability and the gas temperature.

Global (volume-averaged) models [1, 14] are simple but powerful tools to analyse systematic trends. They have less computational load and simulation results are easily analysed compared with spatially resolved hybrid (kinetic-fluid) models [15, 16]. Global models have been employed for a long time in simple [17, 18] and detailed forms of chemical kinetics [10, 19]. Recently, they were compared with various other models, where their validity has been discussed in detail [20, 21], while practical recommendations are also provided [22]. Time-dependent global plasma models can be also used to investigate the effect of power modulation [23]. Good agreement with the measurements is reported in modulated argon plasmas [24, 25], yet benchmarking against measurements is sparse in chlorine plasmas [25]. Here we attempt to fill this gap by providing extensive comparison with experimental data available in the literature.

Thorsteinsson *et al* recently published a series of global model studies of radio-frequency chlorine plasma in continuous [19, 26, 27] and in modulated power input [25], with a modulation period in the microseconds range. In this study, we additionally include spin–orbit-excited chlorine atoms, and we use updated cross-sections for vibrational excitation of molecular chlorine. Heavy particle quenching of the vibrational levels are also incorporated. Furthermore, we extend the modulation period to the millisecond range, for which an ion–ion plasma appears after the power is cut-off.

In this work we investigate an inductively coupled chlorine plasma [28], with focus on the role of the wall recombination probability and the gas temperature. We employ a global model in the investigation that covers both continuous and millisecond scaled modulated power inputs, while comparison with available experimental data is also provided. The simulations are performed using the modular plasma simulation platform Plasimo [29]. We firstly introduce the setup and global model in section 2. The chemical reactions and species are discussed in section 3. Section 4 contains the details about the implementations of the quasi-neutrality constraints and results are presented in section 5.

## 2. Global (volume-averaged) model

Global models concern volume-averaged quantities under the assumption that the sheath length is negligible [1]. For these quantities, particle or energy transport inside the plasma volume is irrelevant and only the net transport at the plasma–sheath boundary is influential. The transport phenomena at the boundary is effectively taken into account, based on a combination of analytic models [14]. This eradicates the computational load due to the transport and allows a significantly larger number of distinct species to be taken into account compared with spatially resolved models.

In the model, we assume that the power is distributed uniformly inside the chamber and the plasma is spatially homogeneous, i.e. the spatial particle profiles do not change significantly compared with their volume averages. We use a two-temperature description: one temperature is assigned to electrons and the other to heavy particles both with the assumption of Maxwellian distribution functions. Governing equations include particle balance equations for various species and the electron energy balance equation; all are integrated over the volume [14]. Particle balance equations determine all particle densities except for the electrons. The electron density is calculated from the quasi-neutrality assumption. This assumption, however, is implemented in different ways for the continuous and modulated power inputs due to faster recombination of electrons compared with millisecond scale modulation periods. The quasi-neutrality implementation in the power modulation is explained in section 4. The electron temperature is derived from the electron energy balance equation, while the heavy particle temperature is provided externally.

### 2.1. Setup

We simulate several different experimental setups composed of cylindrical chambers and particularly the one presented in [28]. In this setup, the plasma forms inside a (hollow) cylindrical chamber with length $L = 1.0 \times 10^{-1}$ m and radius $R = 2.75 \times 10^{-1}$ m. The chamber wall is composed of hard anodized aluminum. Inductive power coupling is realized by an external four-turn planar spiral coil operated at a radio-frequency of $f = 13.56$ MHz. Pure $Cl_2$ gas at $T_{in} = 300$ K is introduced into the chamber with a mass flow rate of $Q = 50$ sccm.

### 2.2. Particle balance equation

For a species $i$, the volume-averaged particle balance equation can be expressed by the relation [14]

$$\frac{dn_i}{dt} = S_i, \tag{1}$$

where $n_i$ is the particle density and $S_i$ is the source. The source is located either inside the plasma or at its boundary. These locations distinctively characterize the nature of the source. Source terms inside the volume are defined by the chemical reactions among the species, whereas at the boundary, they are determined by the chamber wall and the particle transport. In order to denote these two source types, we use the subscripts V and W that symbolize the volume and the wall, respectively. The source includes the reactions, in which the species $i$ is produced and destructed. The former is represented by $\{P\}$

and the latter by $\{D\}$. Based on these notations, the source is written as [19]

$$S_i = \sum_{j\in\{P\}} R_i^j\Big|_{\mathrm{V,W}} - \sum_{j\in\{D\}} R_i^j\Big|_{\mathrm{V,W}}, \tag{2}$$

where $j$ is a particular reaction and $R_i^j$ is the rate of the reaction involving the species $i$.

*2.2.1. Reaction rates.* The volume reactions are composed of the chemical interactions between the individual plasma species, and their rates are distinctively characterized by the reactants. For a volume reaction $j$, the rate is expressed by the relation

$$R^j\big|_V = k^j \prod_l n_i^{\nu_{ji}}, \tag{3}$$

where $k^j$ is the rate coefficient and $\nu_{ji}$ is the stoichiometric coefficient of reactant $i$. The rate coefficient either depends on the electron temperature $T_\mathrm{e}$ or the gas temperature $T_\mathrm{h}$ when all the reactants are heavy particles.

Unlike the volume reactions, the wall reactions are induced by the chamber wall and effectively derived from the particle transport. These reactions are uniquely defined by the particle charge and state. The positive ions recombine at the wall and return back to the plasma as neutrals. On the other hand, the potential drop at the sheath traps most of the negative ions; therefore, their wall losses are negligible. The neutral particles diffuse towards the boundary, where they recombine or de-excite at the chamber wall and return back into the volume. In addition to these processes, the convection due to mass flow carries all the species out of the plasma and feeds the chamber with the input gas.

For a positive ion labelled by p, the ion flux towards the boundary explicitly depends on the density located at the wall $n_p\big|_W$. This wall density is coupled to its volume-averaged equivalent $n_p$ by a ratio $h_p$: $n_p\big|_W = n_p h_p$. Furthermore, it is assumed that the ion reaches the Bohm velocity $u_{Bp} = (eT_\mathrm{e}/m_p)^{1/2}$ at the wall, where $m_p$ identifies the mass. Hence, the ion flux towards the boundary is defined by the expression $n_p h_p u_{Bp}$. With the assumption that every ion that collides with the wall neutralizes, the ion wall loss rate is conventionally expressed by the relation [30]

$$R_p^+\big|_W = u_{Bp} n_p \frac{A_{\mathrm{eff},p}}{V}, \tag{4}$$

where $V$ is the plasma volume, $A_{\mathrm{eff},p}$ is the effective wall area and superscript '+' denotes the positive ions. The effective wall area represents the total plasma surface and embodies the ratio $h_p$, which, in general differs in radial and axial surfaces. For a cylinder, it satisfies

$$A_{eff,p} = 2\pi(R^2 h_{L,p} + LRh_{R,p}), \tag{5}$$

where $h_{L,p}$, $h_{R,p}$ are the axial and the radial edge ratios, respectively.

The ion ratios, $h_p$, are derived from analytic models of electronegative radio-frequency plasmas [30]. According to these models, they are defined by a number of spatial ion profiles, that are combined by an ansatz [22]. As a caveat; the electronegativity modifies the Bohm velocity with respect to the electropositive plasmas [31] and the modification is internally taken into account in the ratios. We adapt the ansatz $h_p = (h_{a,p}^2 + h_{c,p}^2)^{1/2}$ [19], which combines a low-pressure electropositive edge and a flat-topped electronegative profile:

$$\begin{aligned} h_{L,a,p} &\approx \frac{0.86\,(3 + L/2\lambda)^{-1/2}}{1+\alpha_0}, \\ h_{R,a,p} &\approx \frac{0.8\,(4 + R/\lambda)^{-1/2}}{1+\alpha_0}, \\ h_{c,p} &\approx \left(\gamma^{1/2} + \gamma^{1/2} n_{p*}^{1/2} n_p n_-^{-3/2}\right)^{-1}, \end{aligned} \tag{6}$$

where $\gamma = T_\mathrm{e}/T_h$, $\alpha_0 \approx (3/2)\alpha$ is the central electronegativity [10], $n_-$ is the total negative ion density, and

$$n_{p*} = \frac{15}{56}\frac{v_p}{k_{r,p}\lambda}. \tag{7}$$

Here $v_p = (8k_B T_h/\pi m_p)^{1/2}$ represents its mean thermal velocity, where $k_B$ is the Boltzmann constant, and $k_{r,p}$ is the rate coefficient of mutual neutralization with negative ions (reactions 25 and 27 in table 4). The mean free path is

$$\lambda = \frac{k_B T_h}{P\sigma}, \tag{8}$$

where $P$ is the gas pressure and $\sigma$ is the effective scattering cross-section. We set an average value for the cross-section $\sigma = 7\times10^{-19}\,\mathrm{m}^2$ based on [19].

The neutral particles are lost at the boundary due to the outward diffusive flux. Their collisions with the wall provoke reactions that are unique for each species and the consequent products return to the plasma. A superscript $N$ is introduced to represent their rates and for a neutral particle $i$, the wall reaction rate is given by [32, 33]

$$R_i^N\big|_W = n_i\left(\frac{\Lambda_0}{D_i} + \frac{2V(2-\gamma_i)}{A v_i \gamma_i}\right)^{-1}, \tag{9}$$

where $D_i$ is the diffusion coefficient [1], $v_i$ the mean neutral velocity, and $\gamma_i$ is the wall reaction probability. The effective diffusion length $\Lambda_0$ for a cylinder is [33]

$$\Lambda_0 = \left[\left(\frac{\pi}{L}\right)^2 + \left(\frac{2.405}{R}\right)^2\right]^{-1/2}. \tag{10}$$

The mass flux simply feeds the chamber with $Cl_2$ on one side and drains the plasma species on the other. In this respect, the $Cl_2$ flow-in rate is formulated as

$$R_{\mathrm{Cl}_2}^{in}\big|_W = CQ\frac{P_\mathrm{atm}}{Vk_B T_\mathrm{in}}, \tag{11}$$

where $C = 1.6667\times10^{-8}$ is a conversion unit from sccm to $\mathrm{m}^3\mathrm{s}^{-1}$, $Q$ is the mass flow rate in sccm, $P_\mathrm{atm}$ is the atmospheric pressure and $T_\mathrm{in} = 300\,\mathrm{K}$ is the temperature of the input gas. Similarly, a particle $i$ flows out of the chamber at a rate

$$R_i^{\mathrm{out}}\big|_W = CQ\frac{P_\mathrm{atm}T_h}{VPT_\mathrm{in}}n_i. \tag{12}$$

**Table 1.** The power transfer efficiency $\beta$ and gas temperature $T_h$ (K) measurements at various input power $\mathcal{P}$ (W) and pressure $P$ (mTorr).

| Par. \ P | 2 mTorr | 5 mTorr | 10 mTorr | 20 mTorr | 50 mTorr |
|---|---|---|---|---|---|
| $\beta(\mathcal{P}=100)$ | 0.76 | 0.79 | 0.82 | 0.80 | 0.81 |
| $\beta(\mathcal{P}=200)$ | 0.86 | 0.88 | 0.90 | 0.91 | 0.85 |
| $\beta(\mathcal{P}=500)$ | 0.91 | 0.93 | 0.94 | 0.94 | 0.95 |
| $T_h(\mathcal{P}=100)$ | 400 | 450 | 500 | 600 | 600 |
| $T_h(\mathcal{P}=200)$ | 450 | 550 | 650 | 800 | 500 |
| $T_h(\mathcal{P}=500)$ | 550 | 700 | 900 | 1200 | 1100 |

### 2.3. Electron energy balance equation

The electron energy balance equation can be written as [14]

$$\frac{\mathrm{d}p_e}{\mathrm{d}t} = Q_e, \tag{13}$$

where $p_e = 3/2 n_e T_\mathrm{e}$ is the energy density, the right-hand side represents the source and the unit eV is used to describe the electron temperature. The source contains the power absorbed or released by the electronic reactions. Additionally, it includes the loss rate due to elastic electron collisions and absorption of energy, which is applied externally

$$Q_e = Q_\mathrm{abs} - Q_\mathrm{Che} - Q_W - Q_\mathrm{Ela}, \tag{14}$$

where $Q_\mathrm{abs}$ is the absorbed input power, $Q_\mathrm{Che}$ is the chemical loss in the volume, $Q_W$ is the loss at the plasma wall and, $Q_\mathrm{Ela}$ represents the elastic losses within the plasma.

We assume that the electrical energy provided to the chamber is mostly absorbed by the electrons and then distributed to the rest of the plasma species. The electronic reaction energies are either absorbed or released by the electrons, i.e. they are the ultimate energy reservoir in the particle interactions. In view of this, the absorption is written as

$$Q_\mathrm{abs} = \beta\mathcal{P}/V, \tag{15}$$

where $\beta$ is the power transfer efficiency (see table 1) and $\mathcal{P}$ is the input power. The chemical source term $Q_\mathrm{Che}$ contains the electronic reactions in the following

$$Q_\mathrm{Che} = \sum_j \mathcal{E}_j R_e^j \Big|_V, \tag{16}$$

where $\mathcal{E}_j$ is the reaction energy and $R_e^j$ is the reaction rate. The reaction rate is defined in the previous section and the reaction energy represents the net amount of energy absorbed by the reaction. It is the sum of internal energies of the products subtracted from those of the reactants

$$\mathcal{E}_j = \sum_{i\in\mathrm{products}} \nu_{ji}\epsilon_i - \sum_{i\in\mathrm{reactants}} \nu_{ji}\epsilon_i, \tag{17}$$

where $\epsilon_i$ is the internal energy of the particle. The internal energies are shown in the energy diagram figure 10. With the assumption that the electron temperature is much bigger than the gas temperature we define the elastic loss [34]

$$Q_\mathrm{Ela} = \sum_i n_e n_i 3T_\mathrm{e}\frac{m_e}{m_i}k_{ei}^{El}, \tag{18}$$

where $k_{ei}^{El}$ is the elastic rate coefficient and $m_i$ represents the mass of a particle. The elastic rate coefficient is computed from the corresponding collision cross-section and is a function of the electron temperature.

The wall energy losses are due to the positive ions lost by the transport at the plasma boundary

$$Q_W = \sum_{p\in Ions} (\mathcal{E}_e + \mathcal{E}_s + \mathcal{E}_P)\, R_p^+ \Big|_W, \tag{19}$$

where $\mathcal{E}_e = 2T_\mathrm{e}$ is the mean energy loss per electron, $\mathcal{E}_s$, $\mathcal{E}_P$ are the sheath and the plasma potentials, respectively. We use the sheath potential expression [19]

$$\mathcal{E}_s \approx \ln\left(4\frac{\widehat{u_{B'}}}{v_e}\frac{1+\alpha_s}{1+\alpha_s(v_-/v_e)^2}\right)T_\mathrm{e}, \tag{20}$$

where $v_e$ and $v_-$ are the electron and negative ion mean thermal velocities, respectively, $\alpha_s = n_-/n_e|_W$ is the degree of electronegativity at the sheath edge and $\widehat{u_{B'}} = \sum_p n_p u_{B',p}/\sum_p n_p$ is the density weighted positive ion Bohm velocity. The electronegativity changes the Bohm velocity by a factor that is provided by Braithwaite *et al* [31]. Conventionally, this factor is included in the effective area for the ion wall loss rate (see equation (4)). In the sheath potential we explicitly express the factor within the relation

$$u_{B',p} = \left[\frac{eT_\mathrm{e}(1+\alpha_s)}{m_p(1+\alpha_s\gamma)}\right]^{1/2}. \tag{21}$$

The plasma potential for an electronegative plasma is given by [1]

$$\mathcal{E}_P = \frac{1}{2}\frac{1+\alpha_s}{1+\alpha_s\gamma}T_\mathrm{e}. \tag{22}$$

The sheath electronegativity $\alpha_s$ is related to the presheath electronegativity $\alpha_b$ by [14]

$$\alpha_s = \alpha_b \exp\left[\frac{(1+\alpha_s)(1-\gamma)}{2(1+\alpha_s)\gamma}\right]. \tag{23}$$

We employ a fit function for $\gamma > 10$, presented in [19], with the assumption that $\alpha_b$ is equal to the central degree of electronegativity.

### 2.4. Numerical approach

We introduce a vector notation for the sake of simplicity in the numerical implementation. Let $\boldsymbol{n} = \{n_i,\ p_e\}$ be the density vector that includes the particle densities complemented with the electron energy density. Similarly, we define the source vector $\boldsymbol{S} = \{S_i,\ Q_e\}$. By definition the source vector explicitly depends on the density vector and the system of equations takes the form

$$\frac{\mathrm{d}\boldsymbol{n}}{\mathrm{d}t} = \boldsymbol{S}(\boldsymbol{n}). \tag{24}$$

Providing an initial value at time $t_0$, $\boldsymbol{n}(t_0)$, the set is solved iteratively for a variable time-step $\Delta t$ until time $\mathcal{T}$. For the iterative solution, we use the *Livermore Solver for Ordinary Differential Equations* (LSODE) [35]. We set $\mathcal{T}$ large enough for steady-state solutions, i.e. after $\mathcal{T}$ the solution does not change any more.

**Table 2.** The distinct plasma species included in the model. $Cl(^2P3/2)$ is often referred as Cl in this work.

| $Cl_2$ plasma species |
|---|
| $Cl_2$, $Cl_2(v = 0, 1, 2, 3)$, $Cl(^2P3/2)$, $Cl(^2P1/2)$, $Cl(^1P5/2)$, $Cl_2^+$, $Cl^+$, $Cl^-$, $e$ |

**Table 3.** Neutral wall reactions and their probabilities.

| # | Reaction | Probability($\gamma$) | Ref. | Note |
|---|---|---|---|---|
| (1) | $Cl + wall \rightarrow 1/2Cl_2$ | $\gamma_{[A,S]}$ | | See text |
| (2)–(4) | $Cl_2(v) + wall \rightarrow Cl_2(v-1)$ | 1.0 | [26] | |
| (5) | $Cl(^2P1/2) + wall \rightarrow Cl$ | 1.0 | | See text |
| (6) | $Cl(^1P5/2) + wall \rightarrow Cl$ | 1.0 | | See text |

## 3. Chemical model

The set of species, that are contained in the model, are shown in table 2 and the energy diagram is depicted in figure 10 together with the internal energies. Compared with similar chlorine studies [10, 19], we explicitly include the atomic excited levels $Cl(^2P1/2)$ and $Cl(^1P5/2)$. The reactions and the rate coefficients are listed in table 4. The rate coefficients of the electronic reactions are numerically calculated from the corresponding cross-sections with the assumption that the electron energy distribution function is Maxwellian. These numerical data are parametrically fit to functions of the electron temperature.

Most of the fit functions are adapted from a paper by Thorsteinsson *et al* [26], whereas certain rate coefficients are directly computed from the cross-sections (reactions 10, 17, 18, 20, 21 in table 4). A recently updated vibrational excitation cross-section (reaction (10)) by Gregório *et al* [12] is preferred over the one used in the paper [26], since it improves the agreement with experimental observations. The electronic excitation cross-section to level $Cl(^2P1/2)$ (reaction (17)) is calculated by Wang *et al* [13] and to level $Cl(^1P5/2)$ (reaction (18)) by Griffin *et al* [36]. We estimate an ionization rate coefficient from level $Cl(^2P1/2)$ (reaction (20)) based on the electronic Cl ionization (reaction (19)). The ionization cross-section from atomic level $Cl(^1P5/2)$ (reaction 21) and the radiative decay coefficient are taken from [37]. Backward reactions of the excitations are also included in the model by *detailed balancing* [1, 38]. Additionally, the heavy particle quenching reactions (35)–(37) are incorporated. The elastic momentum transfer cross-sections are provided by [36].

The neutral wall reactions are shown in table 3. The Cl recombination probability at a hard anodized aluminum wall has been experimentally determined by Booth *et al* [7]. It depends on the gas pressure and we use an average value for the parameter range in this study

$$\gamma_{A1} = 2.5 \times 10^{-1}, \tag{25}$$

where subscript $A1$ stands for this anodized aluminum measurement. It is also measured by Guha *et al* [5], and lower values are reported that also depend on the $n_{Cl}/n_{Cl_2}$ density ratio. Additionally, such a dependence is also observed for a stainless steel wall by Stafford *et al* [8]. We define these variable recombination probabilities by parametric fits [19]

$$\begin{aligned} \log_{10}(\gamma_{A2}) &= -0.82 - 1.59\exp\left(-1.81\frac{n_{Cl}}{n_{Cl_2}}\right), \\ \log_{10}(\gamma_S) &= -1.22 - 1.34\exp\left(-1.48\frac{n_{Cl}}{n_{Cl_2}}\right), \end{aligned} \tag{26}$$

where $A2$ denotes the aluminum wall measurement by Guha *et al* [5], and $\gamma_S$ is the measurement for the stainless steel by Stafford *et al* [8]. We observe that the plasma is not sensitive to the variations of $Cl(^2P1/2)$ and $Cl(^1P5/2)$ de-excitation probabilities at the wall. Over the range of $Cl(^2P1/2)$ de-excitation probability $10^{-3}-1$ the simulation results, except $Cl(^2P1/2)$ density, change at most with a ratio of 1.09 for the parameters given in table 1. The same variation of the $Cl(^1P5/2)$ de-excitation probability does not alter the results. Consequently, both probabilities are estimated by unity in the simulations.

The wall recombination together with the volume reactions identify the degree of dissociation $\kappa_d = n_{Cl}/(n_{Cl} + 2n_{Cl_2})$. The gas temperature determines the mutual recombination coefficients between the positive and the negative ions. It is also influential on the interactions at the boundary such as ion recombination, neutral reaction rates at the wall and the flow-out rates.

## 4. Quasi-neutrality implementations

For a continuous power input, the electron density is computed from the quasi-neutrality assumption

$$n_e = \sum_i n_i q_i / e, \tag{27}$$

where $i$ represents an ion and $q_i$ is its charge. In the previous global model studies that consider the modulated power input with the modulation periods in the microsecond time-scale [23, 25, 56], the electron density is calculated from the same quasi-neutrality implementation. In these cases, the power modulation periods overlap with the electron recombination time-scale and electrons are still present even at the end of the period.

For larger modulation periods, such as milliseconds, the electrons quickly recombine and vanish in the power-off region. Afterwards, the quasi-neutrality implementation induces non-physical negative electron densities due to the electronegativity. In order to prevent this a different approach is employed to impose the quasi-neutrality. We multiply the particle balance equation of each species with its charge $q_i$, and their summation defines a volume-averaged charge continuity equation:

$$\frac{d\rho}{dt} + \sum_i q_i R_i|_W = 0, \tag{28}$$

where $\rho$ represents the total charge density. The net volume source vanishes due to the charge conservation in the reactions and only the wall flux remains. According to this expression, if initially quasi-neutrality is satisfied, it is further conserved

**Table 4.** The chemical reactions included in the plasma volume (see text). All rate coefficients are in $m^3s^{-1}$, $T_h$ is in K and $T_e$ is in eV unless stated otherwise. The parametric fit range is $T_e = 0.5$–$10$ eV. The backward reactions of the electronic excitations are also included in the model via *detailed balancing*. These excitations are indicated by a letter '*' next to the reaction number. The electronic ionization from $Cl(^2P1/2)$, which is symbolized by '**', is estimated from the electronic ionization of the ground state. The symbol '***' denotes the elastic collisions.

| # | Reaction | Rate coefficient | Ref |
|---|---|---|---|
| (1) | $e + Cl_2(v=0) \rightarrow Cl + Cl + e$ | $1.04 \times 10^{-13} T_e^{-0.29} e^{-8.84/T_e}$ | [39] |
| (2) | $e + Cl_2(v=0) \rightarrow Cl_2^+ + 2e$ | $5.12 \times 10^{-14} T_e^{0.48} e^{-12.34/T_e}$ | [40] |
| (3) | $e + Cl_2(v=0) \rightarrow Cl + Cl^+ + 2e$ | $2.14 \times 10^{-13} T_e^{-0.07} e^{-25.26/T_e}$ | [40, 41] |
| (4) | $e + Cl_2(v=0) \rightarrow Cl^+ + Cl^+ + 3e$ | $2.27 \times 10^{-16} T_e^{1.92} e^{-21.26/T_e}$ | [40, 41] |
| (5) | $e + Cl_2(v=0) \rightarrow Cl + Cl^-$ | $3.43 \times 10^{-15} T_e^{-1.18} e^{-3.98/T_e} +$ $3.05 \times 10^{-16} T_e^{-1.33} e^{-0.11/(T_e+0.014)}$ | [42, 43] |
| (6) | $e + Cl_2(v=1) \rightarrow Cl + Cl^-$ | $14.06 \times 10^{-15} T_e^{-1.18} e^{-3.98/T_e} +$ $12.51 \times 10^{-16} T_e^{-1.33} e^{-0.11/(T_e+0.014)}$ | [42, 43] |
| (7) | $e + Cl_2(v=2) \rightarrow Cl + Cl^-$ | $30.18 \times 10^{-15} T_e^{-1.18} e^{-3.98/T_e} +$ $26.84 \times 10^{-16} T_e^{-1.33} e^{-0.11/(T_e+0.014)}$ | [42, 43] |
| (8) | $e + Cl_2(v=3) \rightarrow Cl + Cl^-$ | $46.31 \times 10^{-15} T_e^{-1.18} e^{-3.98/T_e} +$ $41.18 \times 10^{-16} T_e^{-1.33} e^{-0.11/(T_e+0.014)}$ | [42, 43] |
| (9) | $e + Cl_2(v=0) \rightarrow Cl^+ + Cl^- + e$ | $2.94 \times 10^{-16} T_e^{0.19} e^{-18.79/T_e}$ | [44, 45] |
| (10)* | $e + Cl_2(v=0) \rightarrow Cl_2(v=1) + e$ | $3.99 \times 10^{-12} T_e^{-1.5} e^{-7.51/T_e - 0.0001/T_e^2}$ | [12] |
| (11)* | $e + Cl_2(v=0) \rightarrow Cl_2(v=2) + e$ | $3.28 \times 10^{-17} T_e^{-1.12} e^{-0.37/T_e} +$ $2.86 \times 10^{-17} e^{-(\ln(T_e)+0.99)^2/(2\times 1.06^2)}$ | [46] |
| (12)* | $e + Cl_2(v=0) \rightarrow Cl_2(v=3) + e$ | $1.30 \times 10^{-17} T_e^{-1.24} e^{-0.41/T_e} +$ $6.08 \times 10^{-18} e^{-(\ln(T_e)+0.94)^2/(2\times 1.02^2)}$ | [46] |
| (13)* | $e + Cl_2(v=1) \rightarrow Cl_2(v=2) + e$ | $3.00 \times 10^{-16} T_e^{-1.00} e^{-0.37/T_e} +$ $4.61 \times 10^{-16} e^{-(\ln(T_e)+1.04)^2/(2\times 1.10^2)}$ | [46] |
| (14)* | $e + Cl_2(v=2) \rightarrow Cl_2(v=3) + e$ | $3.00 \times 10^{-16} T_e^{-1.00} e^{-0.37/T_e} +$ $4.61 \times 10^{-16} e^{-(\ln(T_e)+1.04)^2/(2\times 1.10^2)}$ | [46] |
| (15)* | $e + Cl_2(v=1) \rightarrow Cl_2(v=3) + e$ | $1.25 \times 10^{-16} T_e^{-1.13} e^{-0.36/T_e} +$ $1.06 \times 10^{-16} e^{-(\ln(T_e)+1.01)^2/(2\times 1.06^2)}$ | [46] |
| (16) | $e + Cl_2^+ \rightarrow Cl + Cl$ | $9.00 \times 10^{-14} T_e^{-0.50}$ | [19] |
| (17)* | $e + Cl \rightarrow Cl(^2P1/2) + e$ | $4.55 \times 10^{-14} T_e^{-0.46} e^{-2.01/T_e - 0.001/T_e^2}$ | [13] |
| (18)* | $e + Cl \rightarrow Cl(^1P5/2) + e$ | $7.03 \times 10^{-17} T_e^{0.55} e^{-2.15/T_e - 1.5/T_e^2 - 2.05/T_e^3}$ | [36] |
| (19) | $e + Cl \rightarrow Cl^+ + 2e$ | $3.17 \times 10^{-14} T_e^{0.53} e^{-13.29/T_e}$ | [47, 48] |
| (20)** | $e + Cl(^2P1/2) \rightarrow Cl^+ + 2e$ | $3.17 \times 10^{-14} T_e^{0.53} e^{-13.19/T_e}$ | |
| (21) | $e + Cl(^1P5/2) \rightarrow Cl^+ + 2e$ | $4.33 \times 10^{-14} T_e^{0.55} e^{-0.15/T_e - 0.85/T_e^2}$ | [37] |
| (22) | $Cl(^1P5/2) \rightarrow Cl$ | $1.0 \times 10^5 \ \ s^{-1}$ | [37] |
| (23) | $e + Cl^- \rightarrow Cl + 2e$ | $9.02 \times 10^{-15} T_e^{0.92} e^{-4.88/T_e}$ | [49] |
| (24) | $e + Cl^- \rightarrow Cl^+ + 3e$ | $3.62 \times 10^{-15} T_e^{0.72} e^{-25.38/T_e}$ | [49] |
| (25) | $Cl_2^+ + Cl^- \rightarrow 3Cl$ | $5.00 \times 10^{-14} (300/T_h)^{0.50}$ | [1, 50] |
| (26) | $Cl_2^+ + Cl^- \rightarrow Cl + Cl_2$ | $5.00 \times 10^{-14}$ | [51] |
| (27) | $Cl^+ + Cl^- \rightarrow Cl + Cl$ | $5.00 \times 10^{-14} (300/T_h)^{0.50}$ | [1, 50] |
| (28)–(32) | $Cl_2(v=0-3) + Cl^+ \rightarrow Cl + Cl_2^+$ | $5.40 \times 10^{-16}$ | [52] |
| (33) | $2Cl + Cl_2 \rightarrow 2Cl_2$ | $3.50 \times 10^{-45} e^{810/T_h} \ \ m^6s^{-1}$ | [53] |
| (34) | $2Cl + Cl \rightarrow Cl_2 + Cl$ | $8.75 \times 10^{-46} e^{810/T_h} \ \ m^6s^{-1}$ | [54] |
| (35)–(37) | $Cl + Cl_2(v>0) \rightarrow Cl_2(v-1) + Cl$ | $1.3 \times 10^{-17} (T_h/300)^{1/2}$ | [55] |
| (1)*** | $e + Cl_2 \rightarrow Cl_2 + e$ | | [36] |
| (2)*** | $e + Cl \rightarrow Cl + e$ | | [36] |

in time, when the total flux—or the net current—to the wall vanishes

$$\sum_i q_i R_i|_W = 0. \tag{29}$$

Accordingly, we explicitly solve the electron particle balance equation but impose a constraint on its wall flux

$$R_e|_W = \sum_{i \neq e} q_i / e R_i|_W. \tag{30}$$

A caveat about the approach: the numerical integration schemes that use large time-steps can produce deviations.

As the power is switched off, the electron temperature steeply drops in microseconds, together with the plasma and sheath potential. A minimum value for the electron temperature is identified by the gas temperature with the assumption that electrons and background gas are in thermal equilibrium. Afterwards, all the electrons recombine, which is defined by a minimal density condition in the model. The ion wall rates $R_p^+|_W$ that are derived in the presence of the electrons and a power input, are no longer valid and they are switched off. The chemical kinetics, mass flow and the wall flux define an ion recombination time-scale. In case this time-scale is larger than that of electrons, the ions remain in the chamber and they form a quasi-neutral ion–ion plasma.

In the chlorine plasma, the ion recombination time-scales are relatively large and a quasi-neutral ion–ion plasma appears

after the electrons disappear. In this respect, we define two separate regions with respect to time: (1) the plasma, (2) the ion–ion plasma (afterglow). The transition between these regions is defined by a minimal electron density condition. After the electrons disappear, the electron and the ion wall flux rates $R_p^+|_W$ are switched off and only the flow rates and the neutral wall reactions are kept. Similarly, the quasi-neutrality is imposed with negative ion wall flux

$$R_{\mathrm{Cl}^-}|_W = \sum_{i\neq e,\mathrm{Cl}^-} q_i/eR_i|_W. \qquad (31)$$

## 5. Results

In this section, we firstly compare the simulation data with various experimental results obtained from the literature. The comparison covers both continuous and modulated power inputs. Secondly, the simulation results for the recombination probabilities $\gamma_{A1}$, $\gamma_{A2}$ and $\gamma_S$ are compared with each other in the continuous mode. The recombination probability and the gas temperature are varied within a large spectrum to observe their role on the plasma. Finally, their influence on the power modulation is provided at the end of the section.

### 5.1. Experimental comparison

For steady power input we compare the simulation results with the measurements realized by Efremov *et al* [57] and Hebner *et al* [58]. The former are carried out on a setup with a radius of $R = 1.5 \times 10^{-1}$ m, a length of $L = 1.4 \times 10^{-1}$ m at a flow rate of $Q = 20$ sccm and a power input of 400 W. We assume that 300 W is absorbed by the plasma and the gas temperature is $T_h = 500$ K adapted from [19]. The second setup is a cylinder with $R = 5.5 \times 10^{-2}$ m and $L = 3.8 \times 10^{-2}$ m . The mass flow rate is 30 sccm and the power input is fixed at 240 W. For this case, we estimate the $\beta$ factors and the gas temperatures from the measurements listed in table 1 by interpolation. The chamber walls in both setups are composed of stainless steel and the corresponding wall recombination probability, $\gamma_S$, is used in the simulations. The comparisons of the electron, negative ion densities and the electron temperature with respect to the pressure are shown in figures 1(*a*) and (*b*). The simulation results mostly show good agreement with the experimental measurements for these cases. The agreement is fair for the electron density profile at 1.5 mTorr pressure and for the electron temperature profile at 1 mTorr and 25 mTorr.

Sirse *et al* [59] recently measured the $e$, Cl and Cl($^2P1/2$) densities in a setup identical to the one described in section 2.1. We also compare the calculated $e$, Cl and Cl($^2P1/2$) densities at 50 mTorr with these measurements. The comparison is shown with respect to the power input in figure 1(*c*). In general, the results agree well with the experimental data, though the agreement is fair for the excited state density and deviates the most at 100 W.

In pulsed mode we compare the simulation results with the experimental data obtained by Ahn *et al* [60]. The plasma is formed inside a glass Pyrex tube with $R = 1.6 \times 10^{-1}$ m and

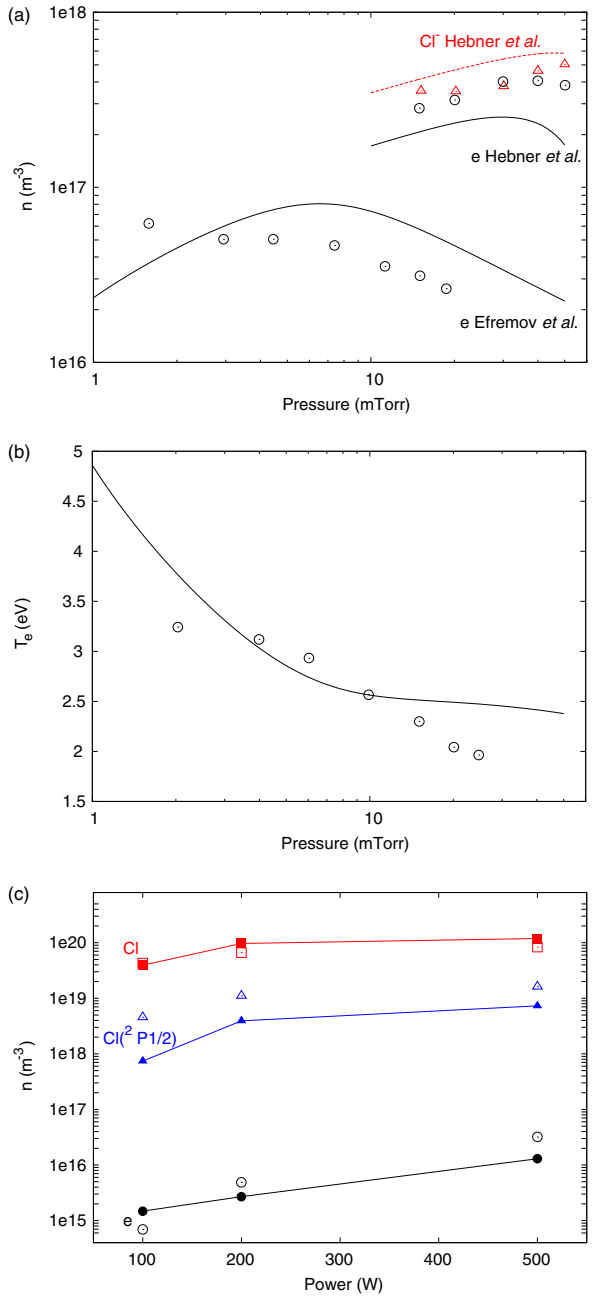


**Figure 1.** Various experimental data (points) measured by Efremov *et al* [57] Hebner *et al* [58] and Sirse *et al* [59] together with corresponding simulation results (lines or line-points). A distinct colour is assigned to each data set. See text for the operation conditions. (*a*) $e$ (○) and $Cl^-$ (△) densities (m$^{-3}$) by Efremov *et al* and Hebner *et al*. (*b*) Electron temperature, $T_e$ (eV), by Efremov *et al*. (*c*) $e$ (○), Cl (□) and Cl($^2$P1/2) (△) densities (m$^{-3}$) by Sirse *et al*.

$L = 1.6 \times 10^{-1}$ m. The power input is 400 W and the pressure is fixed at 8 mTorr. The period of the modulation is 100 $\mu$s with a 50% duty ratio. For the glass wall, we assume a chlorine wall recombination constant of $\gamma_G = 0.15$ proposed by Ashida *et al* [23]. The absorbed power is estimated by a factor of $\beta = 0.9$ based on table 1. The setup is connected to a diffusion chamber with identical gas pressure. Ramamurthi *et al* [3] showed in a similar setup that the plasma does not diffuse into this chamber for the same modulation parameters. Since the

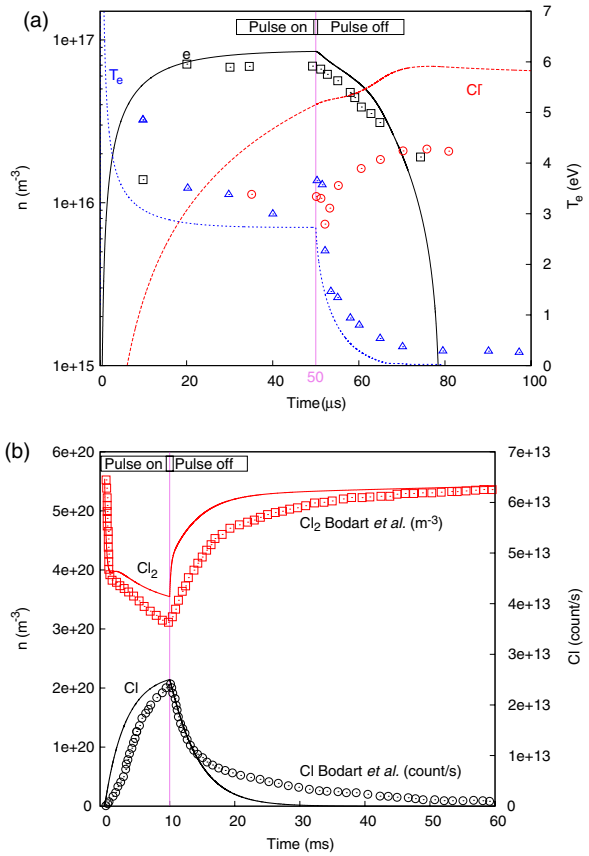


**Figure 2.** Various experimental data (points) by Ahn *et al* [60] and by Bodart *et al* [4] together with the simulation results (lines) in the power modulation. In both graphs the experimental and the numerical results are linked with their colours. See text for the operation conditions. (*a*) The *e* (□), $Cl^-$ (○) densities ($m^{-3}$) and the electron temperature (△), $T_e$ (eV), measurements (at a period of 100 $\mu$s) by Ahn *et al*. (*b*) The measurements (at modulation period of 66 ms) of $Cl_2$ (□) density ($m^{-3}$) and Cl (○) density (count/s) by Bodart *et al*.

period is very small compared with the flow time-scale, we also observed that a mass flow rate of 30 sccm and 0 sccm does not change the calculations. Hence, the plasma expansion into the downstream region directed towards the diffusion chamber is neglected. The electron, negative ion densities and the electron temperature data in one modulation period are shown in figure 2(*a*). Generally, good agreement is observed between the calculations and the measurements. The agreement for the electron density and temperature is valid throughout the modulation period; however, the model proposes a fairly smaller time-scale for the electron temperature decay. The negative ion density measurements deviate from the simulation mostly between 50 and 55 $\mu$s. Since the experimental data are inconsistent by rapid fluctuations at this interval, it is possible that the disagreement is due to the experimental errors.

Bodart *et al* [4] recently measured the atomic and the molecular chlorine densities with a completely different modulation period compared with the previous case. The measurements are carried out for a period of 0.66 ms with a 15% duty ratio. The setup dimensions are identical to the one described in the section 2.1. It is operated at 800 W input power, 20 mTorr pressure, 100 sccm mass flow rate and gas temperature of 800 K. Considering the increment of the factor $\beta$ with the power input (see table 1), we assume that all of the power is absorbed within the plasma. The gas temperature identifies the flow-out rate. If it is not properly defined in the pulse off region, the mass flow drains excessive amount of species from the chamber with the pulse on value of 800 K. Regarding this, we estimate a cooling time-scale about 20 ms that is based on the observations by Cunge *et al* [61, 62]. In this respect, we assume that the gas temperature drops to the ambient temperature in 20 ms. The calculated and the measured data are given in figure 2(*b*) that show good agreement with each other throughout the modulation period. However, the model predicts a fairly smaller decay time-scale in chlorine density compared with the experimental observation.

### 5.2. Wall recombination probability and gas temperature variations

In this section, we fix the power input at 200 *W* and use the setup described in section 2.1 for the analysis. In the simulations we employ the $\beta$ and gas temperature measurements of the setup (see table 1), whenever necessary. We firstly compare the different recombination probability measurements $\gamma_{A1}$, $\gamma_{A2}$ and $\gamma_S$ discussed in section 3. The pressure-resolved densities of electron, Cl and Cl($^2P1/2$) species and the electron temperature for these probabilities are shown in figure 3, together with the experimental data [59]. The measurement, $\gamma_{A1}$, is the largest among the wall recombination probabilities and it is a constant number. However, $\gamma_{A2}$ and $\gamma_S$ vary with the pressure due to different $n_{Cl}/n_{Cl_2}$ ratio. They satisfy $0.006 < \gamma_{A2} < 0.1, 0.003 < \gamma_S < 0.04$ and peak at 2 mTorr, where the $n_{Cl}/n_{Cl_2}$ is relatively larger. Their difference with $\gamma_{A1}$ rises with the pressure. The highest difference is at 50 mTorr, consequently, the corresponding profiles disagree most at this value. This disagreement is more obvious for the Cl and Cl($^2P1/2$) densities, compared with electron density and temperature. Their profiles for these recombination probabilities fairly agree with each other in the presented pressure range.

In order to observe its influence on the plasma, the Cl wall recombination probability is hypothetically varied within the range 0.001–1. In the investigation, we denote this hypothetical probability by $\gamma_{rec}$ covering a pressure range 5–50 mTorr. The particle densities are shown as a function of $\gamma_{rec}$ at 5 mTorr and 50 mTorr pressure in figure 4: (*a*) charged particles at 5 mTorr, (*b*) charged particles at 50 mTorr, (*c*) neutral particles at 5 mTorr and (*d*) neutral particles at 50 mTorr. According to these figures, there are two distinct chemical partitions and corresponding reaction channels with respect to $\gamma_{rec}$ variation. The first partition is composed of excited atomic states and $Cl^+$ that are mainly produced from Cl. The second partition consists of vibrational excited states, $Cl_2^+$ and $Cl^-$ that are dominantly produced from $Cl_2$. Since the wall recombination probability determines the dominant neutral in the plasma, either Cl or $Cl_2$, these two channels respond oppositely to the wall recombination probability.

Generally, the electron density depends on the species from both chemical partitions described above. It directly

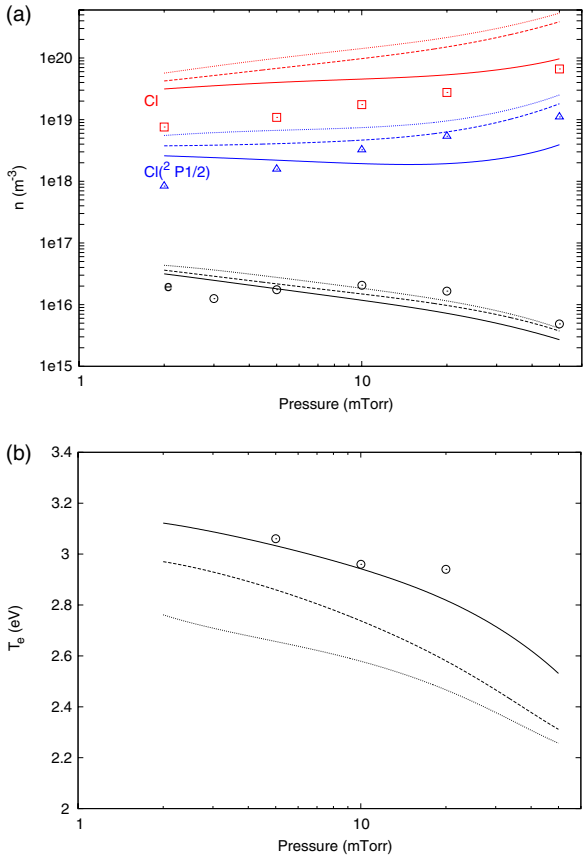


**Figure 3.** Comparison of the electron, chlorine atom and the excited chlorine atom densities and the electron temperature for various recombination probability measurements at 200 W power input. The type of line correspond to each probability: anodized aluminum $\gamma_{A1}$ by [7] (——), anodized aluminum $\gamma_{A2}$ by [5] (- - - -) and stainless steel $\gamma_S$ by [8] (· · · · · ·). The experimental data for the densities and the temperature are provided by Sirse *et al.* [59] for the setup described in section 2.1. (*a*) The electron *e*, Cl and Cl($^2$P1/2) density computations for different recombination probabilities and the measurements. A distinct colour is assigned to each species and the points are measurements: *e* (○), Cl (□) and Cl($^2$P1/2) (△). (*b*) The electron temperature for different recombination probabilities and the measurement.

relies on all the ions in the plasma by the quasi-neutrality requirement and is indirectly determined by the neutrals as the source of the charged particle production. However, the electron density behaves similar to the first partition in the studied parameter range. This is mostly caused by the larger negative ion density that limits the electron density via quasi-neutrality. Otherwise (for example at 500 W), we observe that the electrons behave proportionally to the dominant positive ion. The pressure plays a significant role on the densities and their aforementioned variations. As a consequence, it defines a distinctive behaviour for the electron density together with the wall recombination probability. At a low pressure of 5 mTorr, $Cl^+$ is the dominant positive ion for small $\gamma_{rec}$, whereas the dominant ion switches to $Cl_2^+$ abruptly as $\gamma_{rec}$ increases. At the transition, the electron density shows a slight bump and then decreases with the wall recombination probability. At 50 mTorr, the positive ions are dominated by $Cl_2^+$ in the whole $\gamma_{rec}$ range. Since the negative ions are equally important as the dominant positive ion, the electron density behaviour is mostly identified by $Cl^+$ at this pressure due to quasi-neutrality.

The degree of dissociation $\kappa_d = n_{Cl}/(n_{Cl} + 2n_{Cl_2})$, the degree of electronegativity $\alpha = n_{Cl^-}/n_e$ and the electron temperature $T_e$ variations with respect to $\gamma_{rec}$ are shown in figure 5: (*a*) $\kappa_d$ and $\alpha$ (*b*) $T_e$. The wall recombination probability dramatically reduces the degree of dissociation with a steeper drop at lower pressures. On the other hand, it increases the degree of electronegativity with a similar profile. The electron temperature is almost linearly proportional to $\gamma_{rec}$ for $\gamma_{rec} > 0.02$. Below this point, the relation depends on the pressure. At 5 mTorr and 10 mTorr, the temperature slightly decreases with increasing $\gamma_{rec}$, while at 50 and 20 mTorr the temperature shows an increasing trend. The transition between these two trends corresponds to the dominant ion transition, and the electron density shows a slight bump (see figure 4(*a*)) that causes such an electron temperature behaviour. We observe that the well in the electron temperature for $\gamma_{rec} < 0.002$ deepens for a higher electron density bump (for example at 500 W).

Finally, the influence of the gas temperature on the plasma is investigated by externally varying its value, where the recombination probability $\gamma_{A1}$ is used in the simulations. This can also be physically achievable, for example, by the control of the chamber wall temperature. The resultant particle density profiles are shown in figure 6: (*a*) charged particles at 5 mTorr (*b*) charged particles at 50 mTorr (*c*) neutral particles at 5 mTorr and (*d*) neutral particles at 50 mTorr. The gas temperature variation barely alters the molecular and the negative ion densities. The largest effect on the charged particles is the increase in the electron and $Cl^+$ densities. These behaviours agree with the observations by Thorsteinsson *et al* [19]. The magnitude of the increase at 50 mTorr is significantly larger than the one at 5 mTorr. All the neutral densities are inversely proportional to the gas temperature, which is more apparent at 5 mTorr.

The degree of electronegativity $\alpha$, the degree of dissociation $\kappa_d$ and the electron temperature $T_e$, profiles at different pressure values are shown in figure 7: (*a*) $\alpha$, $\kappa_d$ and (*b*) $T_e$. The gas temperature does not affect the degree of dissociation; however, it decreases the degree of electronegativity with an identical trend for all the pressure values. The electron temperature is almost linearly proportional with the gas temperature regardless of the pressure.

*5.2.1. Power modulation.* In this section, we investigate the role of the wall recombination probability and the gas temperature on the plasma for a modulated power input. In the investigation, a square wave power modulation is applied with a period of 100 ms and a duty ratio of 50% at a 200 W peak power input and pressure 50 mTorr. We use the gas temperature and $\beta$ measurements given in table 1, whenever necessary.

Firstly, we compare four different wall recombination probabilities: $\gamma_{A1}$, $\gamma_{A2}$, $\gamma_{rec} = 0.001$ and $\gamma_{rec} = 1.0$. The corresponding time-resolved charged particles and the electron temperature profiles are shown in figure 8: (*a*) $\gamma_{A1}$, (*b*) $\gamma_{A2}$, (*c*) $\gamma_{rec} = 0.001$ and (*d*) $\gamma_{rec} = 1.0$. Similar $Cl_2^+$ and $Cl^-$

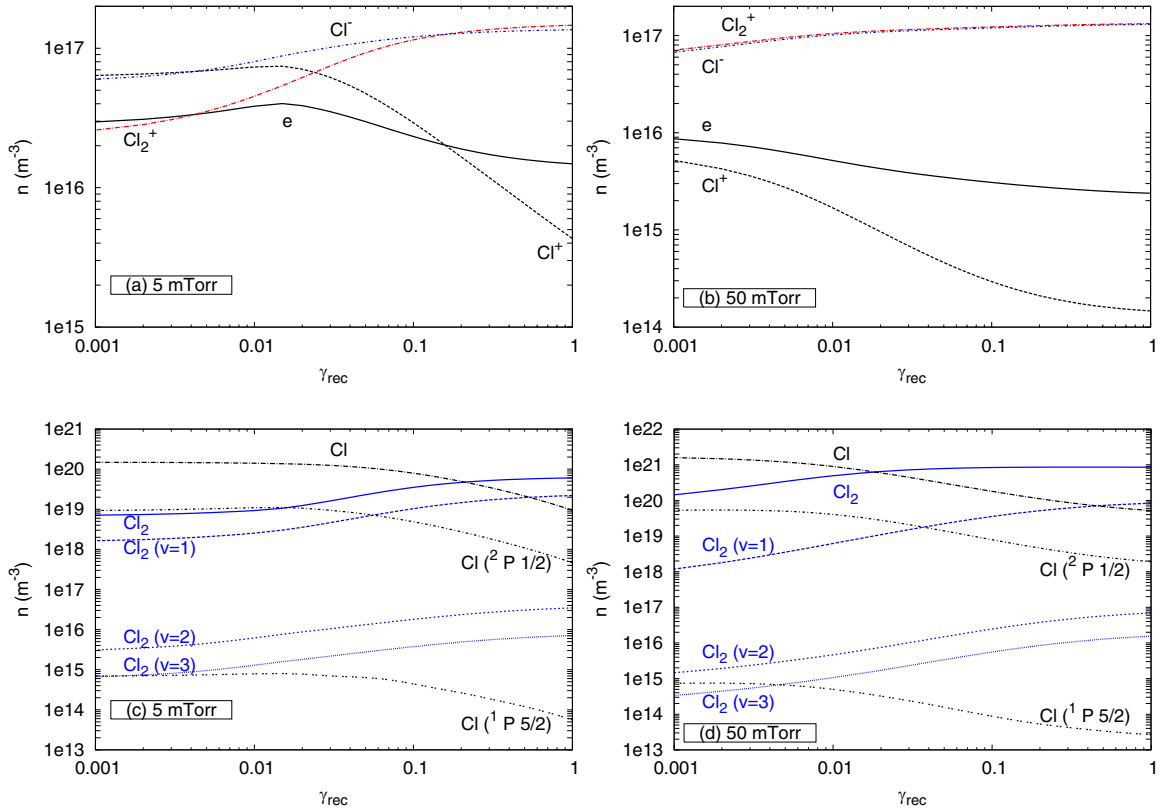


**Figure 4.** The charged and neutral particle densities with respect to the wall recombination probability $\gamma_{\rm rec}$ variation at 200 W power input for the pressure at 5 mTorr and 50 mTorr. (*a*) The charged particles at 5 mTorr and (*b*) at 50 mTorr. (*c*) The neutral particles at 5 mTorr and (*d*) at 50 mTorr.

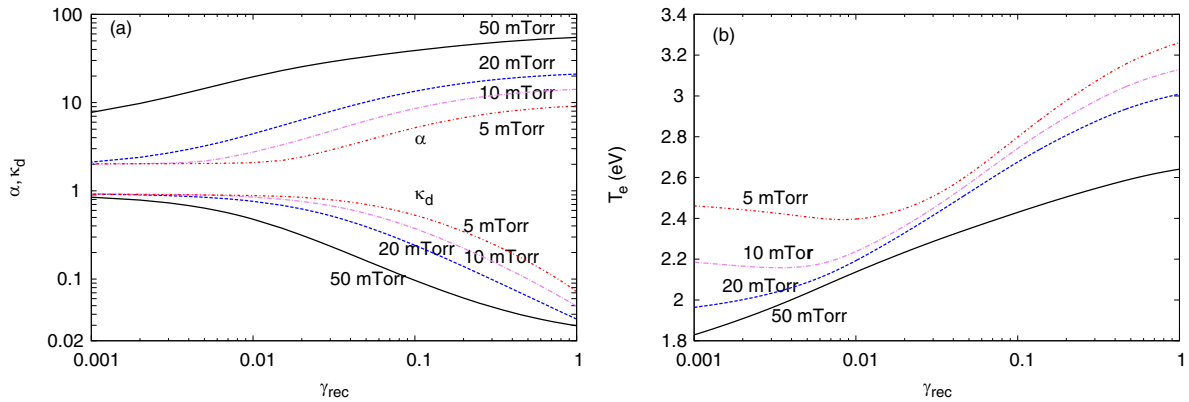


**Figure 5.** (*a*) The degree of electronegativity $\alpha$, dissociation $\kappa_d$ and (*b*) the electron temperature $T_{\rm e}$ with respect to the wall recombination probability $\gamma_{\rm rec}$ variation at 200 W power input.

profiles are observed for the wall recombination probabilities $\gamma_{A1}$ and $\gamma_{A2}$. However, $\gamma_{A2}$ produces larger electron and atomic positive ion densities and slightly lower electron temperatures. The difference is more obvious for the cases of $\gamma_{\rm rec} = 0.001$ and $\gamma_{\rm rec} = 1.0$. For $\gamma_{\rm rec} = 1.0$, the electron temperature and the $Cl^+$ densities are smaller, while the electron temperature is higher. The $Cl_2^+$ and $Cl^-$ profiles do not alter for these two wall recombination probabilities.

Secondly, the comparison of two extreme cases of the gas temperature is shown that are $T_h = 300$ K and $T_h = 1500$ K, respectively, where we employ the recombination probability $\gamma_{A1}$ in the simulations. The resultant charged particle densities and the electron temperature are shown with respect to time in figure 9: (*a*) $T_h = 300$ K and (*b*) $T_h = 1500$ K. The molecular and negative ion profiles are invariant with respect to the gas temperature variation. On the other hand, the electron and $Cl^+$ densities and the electron temperature increase.

In all of the power modulation cases, the electron temperature initially shows a very steep peak due to the low electron density, which is also measured by Ahn *et al* [60]. The quantities during the pulse on are slightly larger than those for the continuous power input. However, the role of the wall recombination probability is identical for the modulated and continuous power inputs that is also observed for the gas

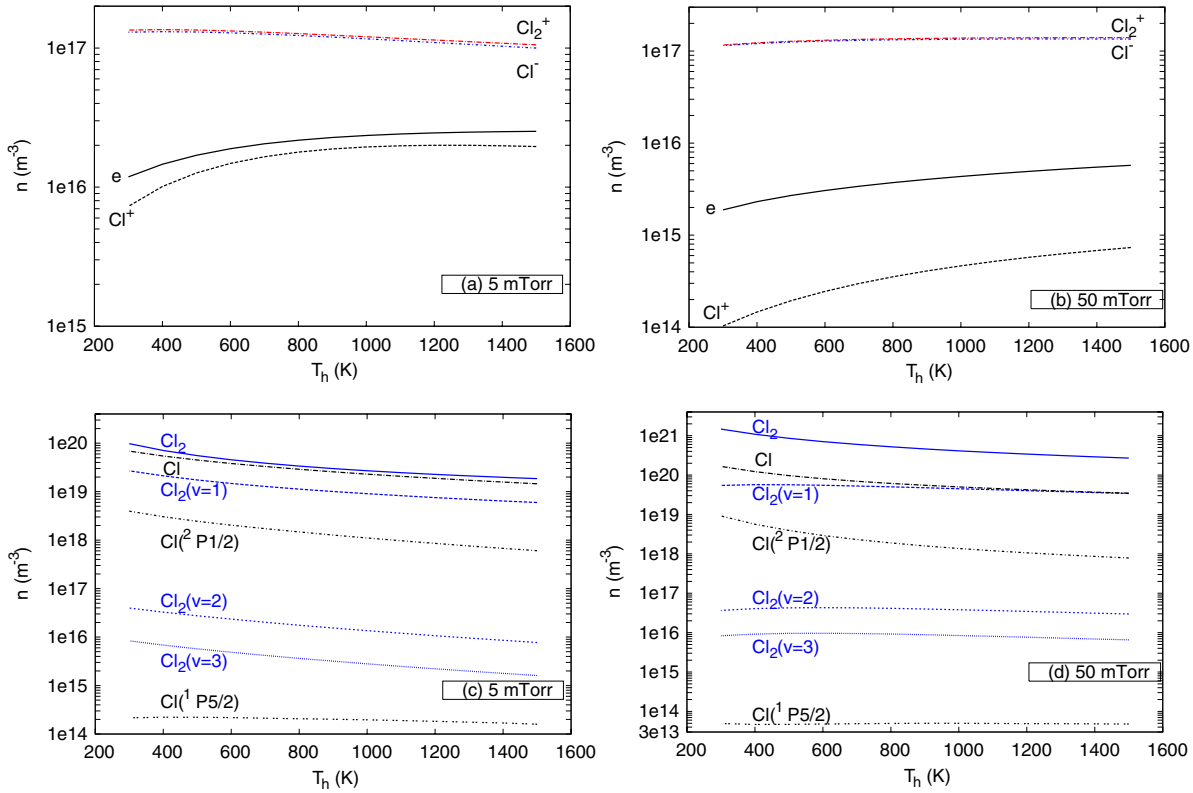


**Figure 6.** The charged and neutral densities with respect to the gas temperature variation at 200 W power input for the pressure at 5 and 50 mTorr. (*a*) The charged particles at 5 mTorr and (*b*) at 50 mTorr. (*c*) The neutral particles at 5 mTorr and (*d*) at 50 mTorr.

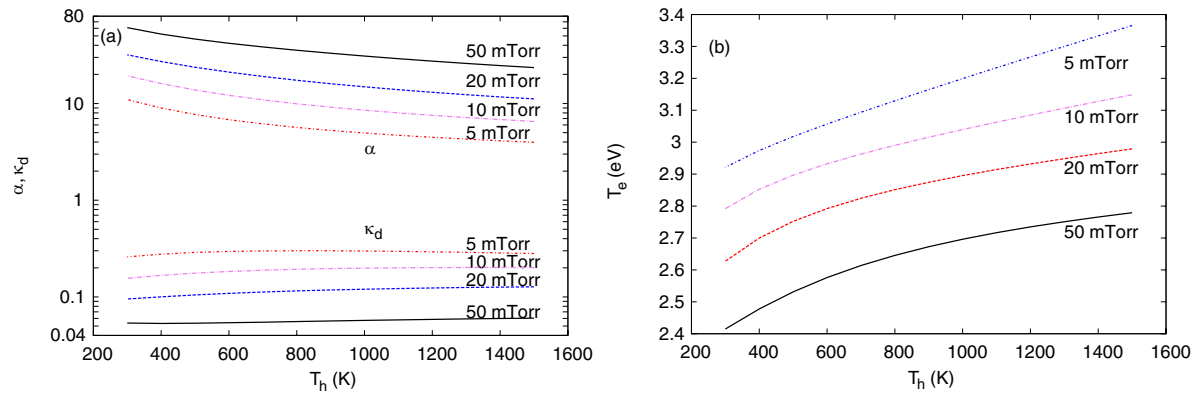


**Figure 7.** (*a*) The degree of electronegativity $\alpha$, dissociation $\kappa_d$ and (*b*) the electron temperature $T_e$ with respect to gas temperature variation at 200 W power input.

temperature. As shown in the continuous case (see figure 4(*a*)), we also observe that at 5 mTorr, $Cl^+$ is the dominant ion at most of the pulse on time for $\gamma_{rec} = 0.001$. As the power is cut-off, the electron temperature and the plasma potential immediately drop within 50 $\mu$s, and shortly after the electrons vanish in the chamber. $Cl^+$ follows the electrons within 200 $\mu$s, which is in an agreement with the observations [2]. Afterwards, an ion–ion plasma that is composed of $Cl_2^+$ and $Cl^-$ appears in the chamber. These ions mutually recombine, as well as they slowly flow out due to the net mass flow rate. The dominant loss mechanism of the ions is initially the mutual recombination then the dominance switches to the flow out rate. In the model we do not set any wall diffusion for these ions, which may lower the ion–ion plasma lifetime.

## 6. Conclusion and discussion

We analysed a chlorine inductively coupled-radio frequency plasma for continuous and modulated power input modes with a global model. The model shows good agreement with the various experimental data from the literature for both power input modes. In the model a novel quasi-neutrality implementation is employed for the power modulation and we observed an agreement with the conventional approach in the pulse on mode. In the pulse off mode an ion–ion plasma composed of $Cl^-$ and $Cl_2^+$ appears in the chamber and the quasi-neutrality is imposed by a similar condition on the negative ion. For an ion–ion plasma composed of multiple dominant negative ions the quasi-neutrality condition is to

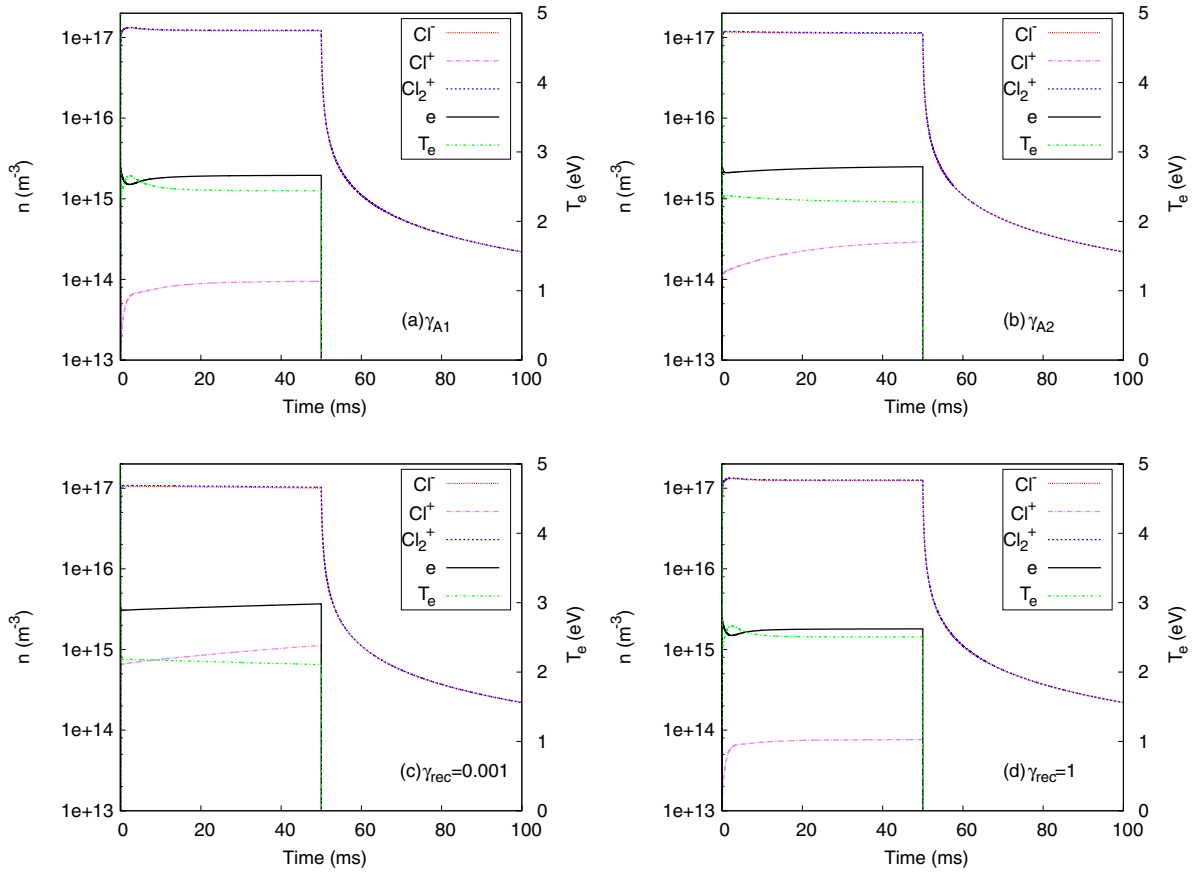


**Figure 8.** Power modulation with period 100 ms and 50% duty ratio at 200 W power input and at 50 mTorr pressure. Each figure shows a different recombination probability (*a*) $\gamma_{A1}$, (*b*) $\gamma_{A2}$, (*c*) $\gamma_{\rm rec} = 0.001$ and (*d*) $\gamma_{\rm rec} = 1$.

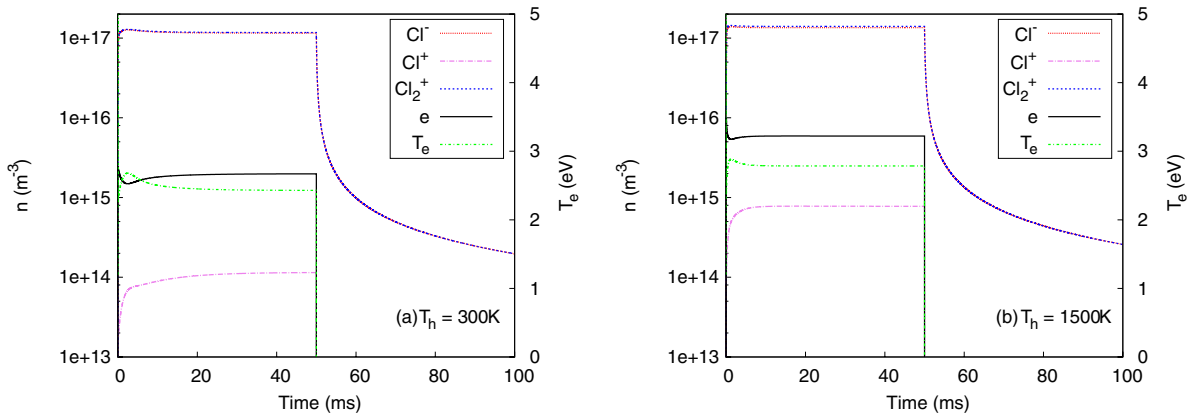


**Figure 9.** Power modulation with period 100 ms and 50% duty ratio at 200 W peak power input 50 mTorr. The figures show (*a*) $T_h = 300$ K and (*b*) $T_h = 1500$ K cases.

be applied to all negative ions, for example, by a density weighted flux.

In the analysis, a comparison of the plasma for distinct measurements of the Cl wall recombination probability is provided. Furthermore, the roles of the wall recombination and the gas temperature variations on the plasma are investigated and it is shown that they have a significant influence. The wall recombination releases energy at the wall and this reaction may directly alter the gas temperature, or indirectly by changing the plasma features. In the model we do not calculate the gas temperature but it is provided externally from measurements. Further analysis with a consistent gas heating requires a model self-consistently coupled to a volume-averaged heavy particle energy balance equation. Additionally, we assume that all the heavy particles are in thermal equilibrium and deviation from this, for example large ion temperature, may alter the influence of the gas temperature.

We observe that the updated vibrational excitation cross-section [12] produces significantly larger $Cl_2(v = 1)$ density compared with the one provided in [46]. On the other hand, the rest of the vibrational excited levels $Cl_2(v = 2, 3)$ do not change and up to date excitation cross-sections are

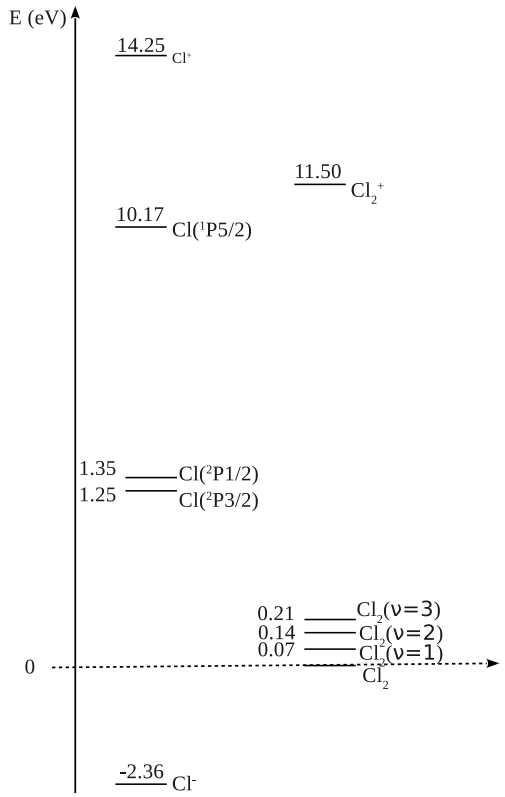


**Figure 10.** Energy diagram of the Cl & $Cl_2$ system. We use the symbol Cl instead of $Cl(^2P3/2)$.

also necessary for these levels. Furthermore, this updated cross-section relatively increases the electron temperature and reduces the electron density; hence, it improves the overall agreement with the experimental data. The quenching reactions of the vibrational levels also play similar role; however, these reactions barely affect the plasma. The influence of the atomic excited chlorine levels is negligible within the parameter range. It is also observed that stepwise ionization from the considered atomic and molecular excited levels are insignificant. Additionally, the plasma is not sensitive to variation of the wall de-excitation probabilities of these excited levels.

## Acknowledgments

This research is supported by the Dutch Technology Foundation STW (project number 10744), and the Draka Comteq Fibre of the Prysmian group (The Netherlands). The work of JPB was performed within the LABEX Plas@par project, and received financial state aid, managed by the Agence Nationale de la Recherche, as part of the programme 'Investissements d'aveni' (ANR-11-IDEX-0004-02). JPB was also supported by the Agence Nationale de la Recherche project INCLINE (ANR-09 BLAN 0019) and by the Applied Materials University Research Partnership Programme. The authors thank Jean-Luc Raimbault and Pascal Chabert for the fruitful discussions on the global models.

## References

[1] Lieberman M A and Lichtenberg A J 2005 *Principles of Plasma Discharges and Materials Processing* (New Jersey: Wiley)
[2] Kanakasabapathy S K, Overzet L J, Midha V and Economou D 2001 Alternating fluxes of positive and negative ions from an ion–ion plasma *Appl. Phys. Lett.* **78** 22–4
[3] Ramamurthi B and Economou D J 2002 Two-dimensional pulsed-plasma simulation of a chlorine discharge *J. Vac. Sci. Technol.* A **20** 467–78
[4] Bodart P, Brihoum M, Cunge G, Joubert O and Sadeghi N 2011 Analysis of pulsed high-density HBr and $Cl_2$ plasmas: impact of the pulsing parameters on the radical densities *J. Appl. Phys.* **110** 113302
[5] Guha J, Donnelly V M and Pu Y 2008 Mass and Auger electron spectroscopy studies of the interactions of atomic and molecular chlorine on a plasma reactor wall *J. Appl. Phys.* **103** 013306
[6] Kota G P, Coburn J W and Graves D B 1998 The recombination of chlorine atoms at surfaces *J. Vac. Sci. Technol.* A **16** 270–7
[7] Booth J P, Sirse N, Chabert P, Azamoum Y and Zaka ul Islam M 2011 Recombination coefficient of Cl atoms on $Al_2O_3$ wall determined by two-photon laser-induced fluorescence *ICPIG-2011 Int. Conf. on Phenomena in Ionized Gases (28 August–2 September 2011)*
[8] Stafford L, Khare R, Guha J, Donnelly V M, Poirier J-S and Margot J 2009 Recombination of chlorine atoms on plasma-conditioned stainless steel surfaces in the presence of adsorbed $Cl_2$ *J. Phys. D: Appl. Phys.* **42** 055206
[9] Cunge G, Sadeghi N and Ramos R 2007 Influence of the reactor wall composition on radicals' densities and total pressure in $Cl_2$ inductively coupled plasmas: II. during silicon etching *J. Appl. Phys.* **102** 093305
[10] Lee C and Lieberman M A 1995 Global model of Ar, $O_2$, $Cl_2$, and Ar/$O_2$ high-density plasma discharges *J. Vac. Sci. Technol.* A **13** 368–80
[11] Meeks E, Shon J W, Ra Y and Jones P 1995 Effects of atomic chlorine wall recombination: comparison of a plasma chemistry model with experiment *J. Vac. Sci. Technol.* A **13** 2884–9
[12] Greg J and Pitchford L C 2012 Updated compilation of electron-$Cl_2$ scattering cross sections *Plasma Sources Sci. Technol.* **21** 032002
[13] Wang Y, Zatsarinny O, Bartschat K and Booth J P 2013 Fine-structure-resolved electron collisions from chlorine atoms in the $(3p^5)^2 P^o_{3/2}$ and $(3p^5)^2 P^o_{1/2}$ states *Phys. Rev.* A **87** 022703
[14] Chabert P and Braithwaite N 2011 *Physics of Radio-Frequency Plasmas* (Cambridge: Cambridge University Press)
[15] Subramonium P and Kushner M J 2002 Two-dimensional modeling of long-term transients in inductively coupled plasmas using moderate computational parallelism: I. Ar pulsed plasmas *J. Vac. Sci. Technol.* A **20** 313–24
[16] Sommerer T J and Kushner M J 1992 Monte Carlo-fluid model of chlorine atom production in $Cl_2$, HCl, and $CCl_4$ radio-frequency discharges for plasma etching *J. Vac. Sci. Technol.* B **10** 2179–87
[17] Rogoff G L, Kramer J M and Piejak R B 1986 A model for the bulk plasma in an RF chlorine discharge *IEEE Trans. Plasma Sci.* **14** 103–11
[18] Richards A D and Sawin H H 1987 Atomic chlorine concentration measurements in a plasma etching reactor: II. A simple predictive model *J. Appl. Phys.* **62** 799–807
[19] Thorsteinsson E G and Gudmundsson J T 2010 A global (volume averaged) model of a chlorine discharge *Plasma Sources Sci. Technol.* **19** 015001

[20] Lazzaroni C, Chabert P, Lieberman M A, Lichtenberg A J and Leblanc A 2012 Analytical-numerical global model of atmospheric-pressure radio-frequency capacitive discharges *Plasma Sources Sci. Technol.* **21** 035013

[21] Monahan D D and Turner M M 2009 On the global model approximation *Plasma Sources Sci. Technol.* **18** 045024

[22] Monahan D D and Turner M M 2008 Global models of electronegative discharges: critical evaluation and practical recommendations *Plasma Sources Sci. Technol.* **17** 045003

[23] Ashida S and Lieberman M A 1997 Spatially averaged (global) model of time modulated high density chlorine plasmas *Japan. J. Appl. Phys.* **36** 854

[24] Lieberman M A and Ashida S 1996 Global models of pulse-power-modulated high-density, low-pressure discharges *Plasma Sources Sci. Technol.* **5** 145

[25] Thorsteinsson E G and Gudmundsson J T 2010 A global (volume averaged) model of a $Cl_2$/Ar discharge: II. Pulsed power modulation *J. Phys. D: Appl. Phys.* **43** 115202

[26] Thorsteinsson E G and Gudmundsson J T 2010 The low pressure $Cl_2/O_2$ discharge and the role of ClO *Plasma Sources Sci. Technol.* **19** 055008

[27] Thorsteinsson E G and Gudmundsson J T 2010 A global (volume averaged) model of a $Cl_2$/Ar discharge: I. Continuous power *J. Phys. D: Appl. Phys.* **43** 115201

[28] Booth J P, Azamoum Y, Sirse N and Chabert P 2012 Absolute atomic chlorine densities in a $Cl_2$ inductively coupled plasma determined by two-photon laser-induced fluorescence with a new calibration method *J. Phys. D: Appl. Phys.* **45** 195201

[29] van Dijk J, Peerenboom K, Jimenez M, Mihailova D and van der Mullen J 2009 The plasma modelling toolkit Plasimo *J. Phys. D: Appl. Phys.* **42** 194012

[30] Kim S, Lieberman M A, Lichtenberg A J and Gudmundsson J T Improved volume-averaged model for steady and pulsed-power electronegative discharges 2006 *J. Vac. Sci. Technol.* A **24** 2025–40

[31] Braithwaite N St J and Allen J E 1988 Boundaries and probes in electronegative plasmas *J. Phys. D: Appl. Phys.* **21** 1733

[32] Booth J P and Sadeghi N 1991 Oxygen and fluorine atom kinetics in electron cyclotron resonance plasmas by time-resolved actinometry *J. Appl. Phys.* **70** 611-20

[33] Chantry P J 1987 A simple formula for diffusion calculations involving wall reflection and low density *J. Appl. Phys.* **62** 1141

[34] Mitchner M and Kruger C H 1973 *Partially Ionized Gases* (New York: Wiley)

[35] Hindmarsh A C 1980 LSODE and LSODI two new initial value ordinary differential equation solvers *SIGNUM Newslett.* **15** 10–11

[36] Griffin D C, Pindzola M S, Gorczyca T W and Badnell N R 1995 Elastic and inelastic scattering of electrons from Ar and Cl *Phys. Rev.* A **51** 2265–76

[37] Tinck S, Boullart W and Bogaerts A 2009 Investigation of etching and deposition processes of $Cl_2/O_2$/Ar inductively coupled plasmas on silicon by means of plasma–surface simulations and experiments *J. Phys. D: Appl. Phys.* **42** 095204

[38] J A M van der Mullen 1990 Excitation equilibria in plasmas; a classification *Phys. Rep.* **191** 109

[39] Cosby P C and Helm H 1992 *Technical Report* WL-TR-93-2004 (US Air Force Material Command Wright Patterson AFB, OH) pp 45433–7650

[40] Basner R and Becker K 2004 Experimental absolute electron impact ionization cross-sections of $Cl_2$ *New J. Phys.* **6** 118

[41] Calandra P, O'Connor C S S and Price S D 2000 Electron-impact ionization of the chlorine molecule *J. Chem. Phys.* **112** 10821

[42] Ruf M, Barsotti S, Braun M, Hotop H and Fabrikant I 2004 Dissociative attachment and vibrational excitation in low-energy electron collisions with chlorine molecules *J. Phys. B: At. Mol. Opt. Phys.* **37** 41

[43] Christophorou L G and Olthoff J K 1999 Electron interactions with $Cl_2$ *J. Phys. Chem. Ref. Data* **28** 131

[44] Kurepa M V and Belic D S 1978 Electron-chlorine molecule total ionisation and electron attachment cross sections *J. Phys. B: At. Mol. Opt. Phys.* **11** 3719

[45] Golovitskii A P 2000 Temperature dependence of an electron attachment to chlorine molecules *Tech. Phys.* **45** 532

[46] Kolorenč P and Horáček J 2006 Dissociative electron attachment, vibrational excitation of the chlorine molecule *Phys. Rev.* A **74** 062703

[47] Hayes T R, Wetzel R C and Freund R S 1987 Absolute electron-impact-ionization cross-section measurements of the halogen atoms *Phys. Rev.* A **35** 578

[48] Ali M A and Kim Y K 2005 Total ionization cross sections of Cl and $Cl_2$ by electron impact *Surf. Interface Anal.* **37** 969–72

[49] Fritioff K, Sandström J, Hanstorp D, Ehlerding A, Larsson M, Collins G F, Pegg D J, Danared H, Källberg A and Le Padellec A 2003 Electron-impact detachment from $Cl^-$ *Phys. Rev.* A **68** 012712

[50] Church M J and Smith D 1978 Ionic recombination of atomic and molecular ions in flowing afterglow plasmas *J. Phys. D: Appl. Phys.* **11** 2199

[51] Lee C, Graves D B and Lieberman M A 1996 Role of etch products in polysilicon etching in a high-density chlorine discharge *Plasma Chem. Plasma Process.* **16** 99–120

[52] Španěl P, Tichý M and Smith D 1993 The reactions of positive and negative halogen ions with $Cl_2$ and $Br_2$ *J. Chem. Phys.* **98** 8660–6

[53] Lloyd A C 1971 A critical review of the kinetics of the dissociation–recombination reactions of fluorine and chlorine *Int. J. Chem. Kinetics* **3** 39–68

[54] Subramonium P 2003 Simulation of transients, transport in plasma processing reactors *PhD Thesis* University of Illinois at Urbana-Champaign

[55] Thompson D L 1974 Monte Carlo classical dynamical study of the Cl + $Cl_2$ and I + $I_2$ systems: vibrational relaxation and atom-exchange reactions *J. Chem. Phys.* **60** 4557

[56] Ashida S, Lee C and Lieberman M A 1995 Spatially averaged (global) model of time modulated high density argon plasmas *J. Vac. Sci. Technol.* A **13** 2498

[57] Efremov A M, Kim G-H, Kim J-G and Kim C-I 2007 Self-consistent global model for inductively coupled $Cl_2$ plasma: Comparison with experimental data and application for the etch process analysis *Thin Solid Films* **515** 5395–402

[58] Hebner G A 1996 Negative ion density in inductively coupled chlorine plasmas *J. Vac. Sci. Technol.* A **14** 2158–62

[59] Sirse N, Booth J P, Chabert P, Surzhykov A and Indelicato P 2013 Chlorine atom densities in the $(3p^5)^2P^o_{1/2}$ excited spin–orbit state measured by two-photon absorption laser-induced fluorescence in a chlorine inductively coupled plasma *J. Phys. D: Appl. Phys.* **46** 295203

[60] Ahn T H, Nakamura K and Sugai H 1996 Negative ion measurements and etching in a pulsed-power inductively coupled plasma in chlorine *Plasma Sources Sci. Technol.* **5** 139

[61] Cunge G, Vempaire D and Sadeghi N 2010 Gas convection caused by electron pressure drop in the afterglow of a pulsed inductively coupled plasma discharge *Appl. Phys. Lett.* **96** 131501

[62] Cunge G, Vempaire D, Ramos R, Touzeau M, Joubert O, Bodard P and Sadeghi N 2010 Radical surface interactions in industrial silicon plasma etch reactors *Plasma Sources Sci. Technol.* **19** 034017